J Comput Aided Mol Des (2013) 27:935–950
DOI 10.1007/s10822-013-9691-1

Mutation effects of neuraminidases and their docking with ligands: a molecular dynamics and free energy calculation study

Zhiwei Yang · Gang Yang · Lijun Zhou

Received: 17 June 2013 / Accepted: 5 November 2013 / Published online: 12 November 2013

Abstract A systematic study has been performed on neuraminidase (NA) mutations and NA-inhibitor docked complexes, with the aim to understand protein–ligand interactions and design broad-spectrum antiviral drugs with minimal resistances. The catalytic D151 residue is likely to mutate while others are relatively conserved. The NA active-site conformations are altered by mutations, but more alterations do not necessarily result in larger deviations to the binding properties. The effects of all related mutations have been discussed; e.g., for the arginine triad (R118, R292 and R371), it is found that residue R118 plays the most significant role during ligand binding. Generally, the calculated binding free energies agree well with the experimental observations. Susceptibility of influenza virus to NA inhibitors can be reinforced by some mutations; e.g., the binding free energies of ligands with N2 subtype increase from -18.0 to -42.1 kcal mol^{-1} by the E119D mutation. Mutations of the various NA subtypes often cause similar conformational and binding changes, explaining the occurrence of cross resistances; nonetheless, differences can be detected in some cases that correspond to subtype-specific resistances. For all NA subtypes, the electrostatic contributions are the major driving force for ligand binding and largely responsible for the binding differences between the wild-type and mutated NA proteins.

Keywords Mutation · Active site · Conformational alteration · Neuraminidase · Drug resistance

Introduction

Over the past century, the Spanish flu (1918–1919), Asian flu (1956–1958) and Hong Kong flu (1968–1969) pandemics deprived millions of lives [1, 2]. Their descendants are continuing to threaten human beings, for example, the 2009 flu pandemic. It has been reported that the surface glycoprotein neuraminidases (NA) of influenza viruses play a significant role during the virus release and replication by selectively breaking the α-glycosidic bond between sialic acid and glycoconjugate [3, 4]. If the NA active sites have been blocked, the virus replication cycle will be interrupted [5, 6]. Accordingly, NAs have ranked as one of the recognized targets for the rational design of antiviral drugs [6, 7].

Oseltamivir (Tamiflu) is the first orally active neuraminidase inhibitor (NAI) that has been widely used for preventing and treating the influenza infections [8, 9]. Oseltamivir carboxylate (OC), the active form of oseltamivir, interacts directly with the NA active-site residues R118, D151, R152, E276, R292 and R371 (according to the N2-subtype numbering [10]); on the other hand, residues E119, D198, I222, H274, E277, N294 and E425 show

Electronic supplementary material The online version of this article (doi:10.1007/s10822-013-9691-1) contains supplementary material, which is available to authorized users.

Z. Yang
School of Basic Medical Sciences, Jiamusi University, Jiamusi 154007, People's Republic of China

Z. Yang · G. Yang
Engineering Research Center of Forest Bio-preparation, Ministry of Education, Northeast Forestry University, Harbin 150040, People's Republic of China

G. Yang (✉) · L. Zhou
Chongqing Key Laboratory of Soil Multi-scale Interfacial Process & College of Resources and Environment, Southwest University, Chongqing 400715, People's Republic of China
e-mail: theobiochem@gmail.com

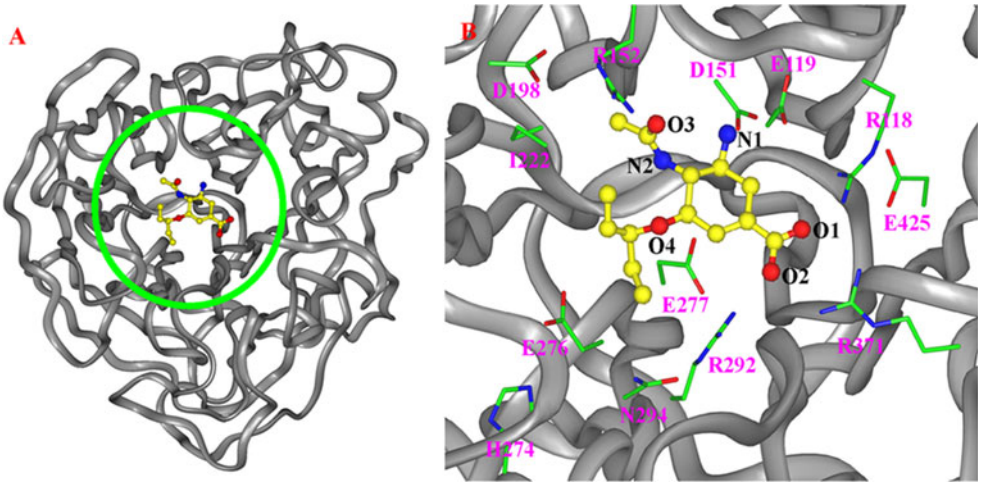

Fig. 1 The complexed structure of oseltamivir carboxylate (*OC*) and the wild-type N2 protein ($N2^{WT}$): **a** ribbon structure and **b** key residues in the active site. R118, D151, R152, E276, R292 and R371 are catalytic residues that have direct interactions to OC. Residues E119, D198, I222, H274, E277, N294 and E425 are implicated to show stabilization effects to the NA active sites. The C, N, O atoms are colored in *yellow*, *blue* and *red* for the OC ligand whereas in *green*, *blue* and *red* for the N2 active-site residues, respectively

stabilization effects to the docked complexes by impacting on the above active-site residues (Fig. 1). Mutations of these residues may significantly affect the binding properties [11–15]. As a matter of fact, the broad screening for the susceptibility of influenza viruses has already detected OC-resistant NA variants. For the N2-subtype, the resistance motions are mainly limited to the conserved active-site residues, see Scheme 1 [11, 16–18]. The mutagenesis was assumed to cause conformational changes to proteins, which further results in drug resistances [11, 16, 18, 19].

Up to date, nine serotypes of NA (N1–N9) belonging to influenza A have been known in avian and mammalian hosts, whereas only type B has been identified for influenza B [7]. The NAs of influenza A can be phylogenetically categorized into Group 1 (N1, N4, N5 and N8) and Group 2 (N2, N3, N6, N7 and N9) [6]. Group 1 differs from Group 2 by having the "150-cavity" adjacent to the NA active site that is formed with loop residues 147–152 [20]. No systematic computational studies have been carried out on the mutations of these NA proteins. It remains ambiguous how the mutations affect the NA conformations, enzymatic activities and OC binding properties. In addition, we are not aware why the OC resistances are subtype-specific; e.g., the E119D/V/A/G and R292K mutations occur mainly in the N2- and N9-subtypes, while E119G, D198N and R152K mutations mainly in the B type [11, 15–19]. These issues are significant to comprehend the protein–ligand interactions and drug-resistance mechanisms as well as design the potent broad-spectrum NAIs with minimal resistances [5, 6, 11]. To this end, this work was outlined as follows: (1) 10 ns molecular dynamics (MD) simulations within explicit water solvent were performed on the wild-type and mutated N2-subtype NA proteins in order to study the mutation effects on their conformations. Potential mutations were listed in Scheme 1; (2) Docking and 10 ns MD simulations within explicit water solvent were performed on the N2–OC complexes of wild-type or mutated; (3) The Molecular Mechanics–Poisson–Boltzmann/Surface Area (MM/PBSA) method was used to predict the free binding energies and rationalize the computational results; (4) 10 ns MD simulations within explicit water solvent were performed on the wild-type and mutated N1-, N9-subtypes and B-type NA proteins; (5) Docking and 10 ns MD simulations within explicit water solvent were performed on N1-, N9-subtypes and B-type NA proteins, finding the similarities and differences among the various NA subtypes.

Methodology

System preparation

The crystal structures of the N1- (2HTY [21]), N2- (1IVD [10]), N9- (1F8B [22]) subtype and B-type (1A4Q [23]) NA proteins, downloaded from the RCSB Protein Data Bank, are high-resolution and possess well-defined active sites. The calcium ion (Ca^{2+}) and water molecules near the active sites play a significant role and accordingly were reserved during the docking and MD simulations [24–27]. The mutations were constructed by replacing the corresponding amino acids using the Biopolymer module (InsightII 2005). All the NA proteins were saturated with hydrogen atoms, based on the expected charge distributions

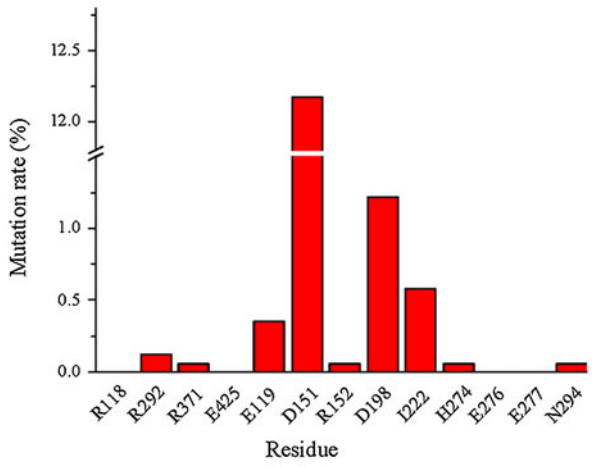

The mutated N2 proteins and their sources

	Source [a]
WT	AY209929 (PDB ID: 1IVD)
R118K	RG
R292K	AY643089
R371K	RG
E425G	HM144629
E119D	RG
E119V	RG
E119A	RG
E119G	CY045814
D151E	RG
D151N	CY032479,CY032495,CY013242,CY013399, CY032447,GU907119,CY039441,CY038513
R152K	CY038484,CY038468
R152I	FJ534539
D198N	CY011130,CY001479,CY009670,AF251396,CY015750,CY009742
I222V	CY035224
H274Y	RG
E276D	RG
E277G	RG
N294S	In clinic

[a] The mutations were rescued by the reports of *in vivo* inhibitor treatment, reverse genetic (RG) or the Influenza Research Database (IRD).[18]

Scheme 1 The mutation rates of the key residues in the N2 active site. The accompanying table gives the sources. The mutation rates were evaluated with the aid of the Influenza Research Database (*IRD*)

of amino acids at physiological pH [24–28]. Then they were energy-minimized by 500-step steepest descent minimization and conjugate gradient minimization until convergence to 0.01 kcal mol^{-1} $Å^{-1}$.

The energy-minimized NA proteins (wild type and mutated) were further equilibrated by 10 ns MD simulations, using the GROMACS4.0.5 program [29] and OPLSAA force field [30–32]. Each protein was immersed into a SPC (simple-point-charge) water box, with the distance from the protein surface to box edge of at least 9.0 Å (about 16,000 water molecules) [32]. The positive charges of the NA proteins were balanced by Cl^- anions [33]. The NPT ensemble (constant pressure and constant temperature) was applied (300 K, 1 Bar) [34] and the long-range electrostatics was described by the particle-mesh Ewald (PME) method [35]. The coulomb and vdW cutoff radii were set to 8.0 and 14.0 Å, respectively. The covalent bonds involving hydrogen atoms were constrained with the LINCS algorithm [36]. The time step was set to 2 fs. The MD trajectories were collected every 10 ps. The NA proteins that have been sufficiently equilibrated were ready for the latter docking studies [32, 37].

Docking and MD simulations

In accord with the previous works [24–27], the docking simulations were performed using the general protocols of InsightII 2005 software package [38], and the ligand plus a sphere with radius of 10.0 Å was allowed to move freely. That is, the protein residues that fall within this region were treated flexible as the ligand. The OC ligand was optimized at B3LYP/6-31G(d,p) level of theory using Gaussian03 program [24, 27, 39, 40]. Then the Affinity module (InsightII 2005), combining Monte Carlo (MC) and simulated annealing (SA) methods, was used to probe the optimal docked complexes, on basis of binding energies and geometrical matching qualities. The protein–ligand complexes, solvated in a sphere of TIP3P water molecules [41], were sufficiently equilibrated by 10 ns MD simulations using GROMACS4.0.5 program [29] and GROMOS96 43a1 force field [42], as recommended elsewhere [24, 32, 37]. The non-bonded interactions were considered by the cell-multipole approach. The average structures of the 5–10 ns MD trajectories were used for structural analysis. The backbone root-mean-square deviation (RMSD), root mean squared fluctuation (RMSF) per residue Cα, and solvent accessible surface areas (SASA) were performed with the built-in analysis tools of GROMACS4.0.5 program [29].

Binding free energies

The binding free energies of the docked complexes (ΔG_{bind}) were calculated using the MM/PBSA method (Amber11 software) [43, 44]. Each docked complex was immersed in a TIP3P water box of 81 × 81 × 81 $Å^3$. As instructed, the ESP charges of OC were derived at B3LYP-IEFPCM/cc-pVTZ//HF/6-31G(d,p) level of theory [39, 45]. In order to compute the binding free energies (ΔG_{bind}), 1 ns production MD trajectories (constant pressure and constant temperature, NPT ensemble) using the ffamber03 force field [13, 45–48] were conducted on the OC–NA complexes that have been equilibrated by 10 ns MD simulations, see "Docking and MD simulations" section. A time step of 2 fs was used and the snapshots were archived every 4 ps for the enthalpy estimates. The exterior and interior dielectric constants (ε) were set to 80.0 and 1.0, respectively. Owing to the prohibitive computational cost, the entropic contributions ($T\Delta S$) were usually not

considered; in addition, the entropic contributions ($T\Delta S$) are expected to be similar for the present investigated NA structures and therefore can be neglected. According to the MM/PBSA approach, the binding free energies (ΔG_{bind}) were decomposed,

$$\Delta G_{bind} = G_{complex} - G_{protein} - G_{ligand} \quad (1)$$

$$= \Delta E_{MM} + \Delta G_{sol} - T\Delta S \quad (2)$$

where $G_{complex}$, $G_{protein}$ and G_{ligand} are the free energies of the docked complex, NA protein and OC ligand, respectively.

ΔE_{MM} represents the molecular mechanical (MM) contribution and is divided into electrostatic (ΔE_{ele}) and van der Waals (ΔE_{vdW}),

$$\Delta E_{MM} = \Delta E_{ele} + \Delta E_{vdW} \quad (3)$$

The solvation free energy (ΔG_{sol}) is divided into polar and nonpolar portions,

$$\Delta G_{sol} = \Delta G_{PB} + \Delta G_{sur} \quad (4)$$

$$\Delta G_{sur} = \gamma SASA + b \quad (5)$$

The polar term (ΔG_{PB}) was derived from the PB calculations using the PBSA module, with the recommended radii and atomic charges [45, 47, 48]. The nonpolar solvation term (ΔG_{sur}) was calculated using the solvent-accessible surface area (SASA) and two empirical parameters, γ (0.00542 kcal mol^{-1} Å^{-1}) and b (0.92 kcal mol^{-1}) [49].

In addition to the default 1 ns MD simulations, 5 ns MD simulations were also performed to calculate the binding free energies (ΔG_{bind}) of the wild-type (OC–N2^{WT}) and two randomly selected mutations (OC–N2^{R292K} and OC–N2^{R371K}), corresponding to three different conditions [50–52]: (a) The same as in the default 1 ns MD simulations; (b) The explicit water model is used as a part of receptors and c) The interior dielectric constant (ε_{in}) is set to 2.0 instead of 1.0. Then the entropic contributions ($T\Delta S$) that were derived from the normal-mode analysis [51] were evaluated for these three docked systems; i.e., OC–N2^{WT}, OC–N2^{R292K} and OC–N2^{R371K}.

Results and discussion

The mutagenesis analysis

In the previous work [26], a multiple sequence alignment has been made for the N1-, N2-, N9-subtype and B-type NA proteins. It shows the active-site residues are rather conserved. Especially, the N2 and N9 subtypes have approximately 50 % sequence identity and their key active-site residues are exactly the same. A number of residues in the NA active sites are directly involved in the interactions with ligands [5, 6, 53]. The arginine triad (R118, R292 and R371) shows electrostatic and H-bonding interactions with the OC carboxylate anion and residue E425 scaffolds the three catalytic residues (Fig. 1). The catalytic residues D151 and R152 form H-bonds with the OC amino-N1 and *N*-acetylamino-N2/O3 atoms, and the former is stabilized by residue E119. Residue E276 undergoes conformational rearrangement in order to match the bulky side chain of OC. The other important residues in the NA active sites can be D198, I222, H274, E277 and N294, which support the above catalytic residues during interactions with ligands through the salt-bridge and hydrophobic effects [19]. Influenza virus variants with mutations of these residues have recently been isolated in vivo and in vitro [11, 16–19, 54–60].

Among the NAs of influenza A, the N1 and N2 subtypes are found to be responsible for the outbreak of pandemics and annual recurrence. Especially, the N2 subtype has been widely spread in the human species [6, 7]. The mutation rates of the above active-site residues have been evaluated for the N2 subtype, with the aid of platform in Influenza Research Database (IRD) [18, 61]. The catalytic residues R118, R152, E276, R292, R371 and framework residues E119, D198, I222, H274, E277, N294, E425 are relatively conserved with their mutation rates below 1.2 %, whereas the catalytic residue D151, which was previously thought to be conserved [62], corresponds to a much higher mutation rate of 12.2 %, see Scheme 1.

The MD simulations show that the wild-type N2 protein quickly arrives to its equilibrium state (Figure S1), consistent with the previous results [24–27, 47, 48, 63]. The backbone RMSD curve reaches a plateau at approximately 0.5 ns and no observable fluctuations are detected afterwards. However, the mutated N2 proteins will not be equilibrated until about 5 ns. This is also applicable to the other NA subtypes (B type and N1, N9 subtypes), see Figure S2. It indicates that the mutations cause rigorous alterations to the NA conformations and thus require sufficiently longer time to adjust and equilibrate. As suggested by the SASA, the N2 active sites shrink in the R118K, E119G, R152I, D198N, E276D, N294S, R371K and E425G mutations whereas expand in the E119D/V/A, D151E/N, R152K, I222V, H274Y, E277G and R292K mutations (Table 1) [64, 65]. Note that the SASA clustering is calculated by comparison with the wild type, on a subset of the 18 residues that cover the entire NA active-site area; i.e., residues 118–119, 151–152, 178, 179, 198, 222, 224, 227, 274, 276–277, 292, 294, 371, 406 and 425 (according to N2 numbering) [53, 66]. N2^{R371K} and N2^{H274Y} correspond to the largest negative and positive SASA alterations, equal to −69.3 and 47.7 Å^2, respectively. As a result of the conformational alterations, the binding properties of the mutated NA proteins are expected to be distinct from the wild types.

Table 1 The relative solvent accessible surface areas (SASA) of the mutated N2 and N2–OC active sites as well as H-bonding information in the N2–OC complexes

	SASA relative to WT		The active-site residues that form H-bonding with OC[a]
	N2	N2–OC	
WT	0.0	0.0	R118(1), D151(1), R152(1), R292(1), R371(2)
R118K	−44.8	−17.2	(0)
E119A	4.7	−37.7	D151(2)
E119D	22.5	−16.6	D119(1)
E119G	−45.5	6.5	E277(3)
E119V	27.9	108.2	(0)
D151E	1.5	36.5	(0)
D151N	12.4	76.5	N151(1), D198(1)
R152I	−18.2	−29.6	E119(1), R371(1), E425(1), R430(2), K431(2)
R152K	26.7	−28.1	E227(3), R292(1)
D198N	−8.4	20.7	E119(2)
I222V	18.1	−28.3	R292(1)
H274Y	47.7	−26.5	R118(3), D151(1), R292(1), Y406(2)
E276D	−59.9	23.0	E119(2), S179(1), E277(2), R371(1), Y406(2)
E277G	14.1	27.2	(0)
R292K	27.6	−81.0	R119(1)
N294S	−22.3	54.9	R118(3), E119(1), D151(1)
R371K	−69.3	−97.7	S245(1), E276(2)
E425G	−16.6	97.4	E119(1), E277(1), Y406(2)

A subset of 18 residues (118–119, 151–152, 178, 179, 198, 222, 224, 227, 274, 276–277, 292, 294, 371, 406 and 425) is used to calculate the SASAs (according to N2 numbering), with the SASA unit of Å^2

[a] The numbers of H-bonds are given in parentheses and (0) indicates no H-bonds

Docking to the wild-type and mutated N2 proteins

As discussed above, all the docked complexes (wild-type and mutated) have been sufficiently equilibrated at 5 ns, and accordingly the average structures of 5–10 ns MD trajectories will be used for analysis. Owing to mutations, the binding properties of N2–OC differ from that of the wild type (N2^{WT}), especially for R118K, E425G, E119D, E119V, D151N, R152K, D198N, H274Y, E276D, E277G and N294S (Fig. 2). Among these mutated cases, the OC–N2^{R371K} and OC–N2^{E119V} active sites are the most altered being the smallest and largest, and their SASA values differ from the wild type by −97.7 and 108.2 Å^2, respectively (Table 1). The alterations of the N2 active-site surfaces further affect the binding properties; nonetheless, the largest SASA changes do not necessarily lead to the greatest deviations to the binding properties. For example, the active site of OC–N2^{R118K} shrinks by 17.2 Å^2 and is less than that of OC–N2^{R371K} (97.7 Å^2), but the deviation of OC orientation is obviously larger and ranks the first among these mutations (Table 1; 2a). Owing to the mutations, the H-bonding interactions of the NA active sites with OC are seriously impaired, especially OC–N2^{R371K} and OC–N2^{E119V} which by coincidence correspond to the largest SASA alterations (Table 1).

Figures 3 and S4 show that as compared to the wild type, mutations can cause larger conformational fluctuations and instability to the key active-site residues; e.g., residue R152 has rather large conformational instability in almost all the mutations. In the wild type, the arginine triad (R118, R292 and R371) forms strong H-bonds with the OC carboxylate anion, as demonstrated by the structural analysis of NA-ligand complexes [11–17]. On basis of the mutation rates of the N2 background (Scheme 1), residue R292 should be the most likely to be mutated among the three arginines, while residue R118 plays the most important role during interaction with OC [16, 64, 67]. In N2^{R118K}, the relative positions and side chain orientation of the arginines in the triad are rigorously disrupted, and their C_ζ atoms shift by 7.5, 4.5 and 8.6 Å, respectively (Fig. 4a). The salt bridge between the R118 guanidino group and the E425 carboxylate anion [16, 64, 67] has been destroyed (Figure S6A), which is consistent with the crystallographic coordinates reported by Yen et al. [19]. As compared to the wild type, OC moves far from the N2 active site with its all-atom RMSD of 24.1 Å (Figure S5); meanwhile, all the H-bonds have vanished (Table 1). This explains why the R118K mutation decreases significantly the enzymatic activity. Instead, the R292K and R371K mutations result in relatively slighter effects, and the ligand-RMSD values are calculated to be 4.9 and 3.3 Å, respectively, with the OC carboxylate anions still interacting with the region as in the wild type (Figure S5). The E425G mutation affects greatly the arginine triad accompanied with high RMSFs and large C_ζ shifts (Fig. 4b). As a result, the OC carboxylate anion orients towards residue Y406 along with the formation of two new H-bonds (Table 1). These are quite distinct from the wild type but can find supporting results from the crystallographic structures [19, 64, 68–70]. The E425G mutation weakens the OC binding [5, 6, 53] and causes slight resistances, which is in agreement with the results of the sensitivity assays (IC_{50} values) [69].

The E119D/V/A/G mutations have been detected in influenza A or B viruses [11–17]. The MD simulations show that the OC orientations in N2^{E119D}, N2^{E119V}, N2^{E119A} and N2^{E119G} are different from the wild type (Fig. 2b), as detected in the crystallographic structures [71–73]. The ligand-RMSD values amount to 8.6, 5.0, 4.2 and 6.1 Å, respectively (Figure S5). Residue D151 functions as an acid catalyst in the sialyl-enzyme intermediate [19, 74], while the E119D/V mutation decreases the

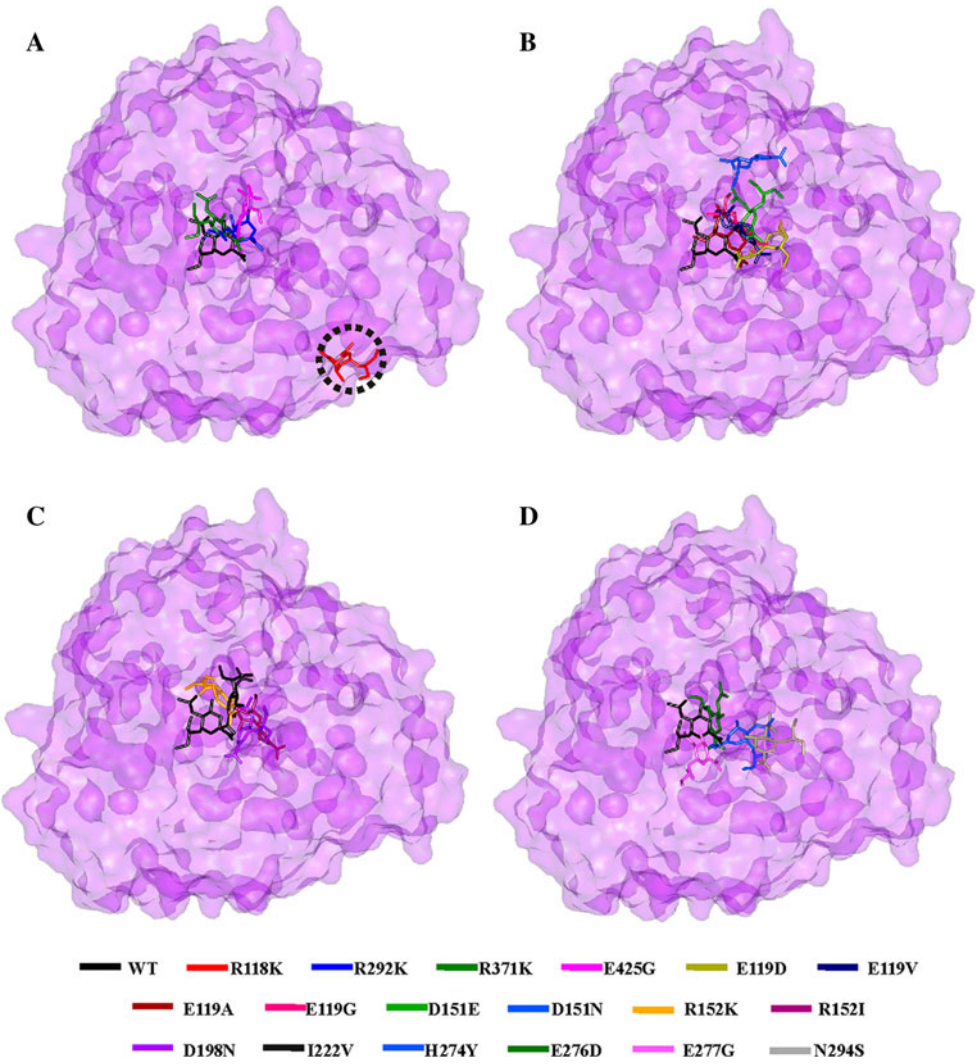

Fig. 2 Superimposition of the OC structures within the wild-type ($N2^{WT}$) and mutated proteins: **a** $N2^{R118K}$, $N2^{R292K}$, $N2^{R371K}$, $N2^{E425G}$, **b** $N2^{E119D/V/A/G}$, $N2^{D151E/N}$, **c** $N2^{R152K/I}$, $N2^{D198N}$, $N2^{I222V}$ and **d** $N2^{H274Y}$, $N2^{E276D}$, $N2^{E277G}$, $N2^{N294S}$. The Connolly surfaces of $N2^{WT}$ (in *purple*) are created using the InsightII 2005 scripts. The OC ligands are represented by *stick* models

conformational stability to a certain degree, see the RMSF plot in Fig. 3; meanwhile, its C_ζ shift amounts to 6.3/10.6 Å (Fig. 5). This indicates that the negative charges (E vs. V/A/G) and suitable lengths of the side chain (E vs. D/V) of residue E119 are crucial to stabilize residue D151. At the same time, the E119D/V mutation causes the C_ζ atom of residue R118 to move by 5.8/3.4 Å (Figure S6). The important role of D151 during ligand binding is further testified by the D151E/N mutation, wherein the SASA value of the NA active site, H-bonding with ligand has been affected (Table 1). As observed in our MD simulations, the D151E/N mutation causes changes in both orientation and distance of R118 carboxylate anion, with the C_ζ shift of 4.9/1.7 Å (Figure S7); nonetheless, the salt bridge between the arginine triad and OC carboxylate anion is maintained. The mutation site D151 (E/N) may form through its side chain the salt bridge with the adjacent residues (e.g., R152, see Figure S7), and the OC binding is altered, with the ligand-RMSD value of 8.0/13.4 Å (Figure S5). This agrees with the residue rearrangements observed experimentally [19, 75] and can also elucidate the virus growing and enzymatic activity results [19, 62, 76].

Our MD simulations show that residue D198 of the wild-type N2 or B has interaction with residue R152, which is disrupted due to the R152K mutation and further causes residue 152 to deviate from the active site center. Thus, the H-bonds with the OC acetamide group will disappear (Table 1), and the ligand-RMSD equals 6.4 Å (Figure S5). It has been reported that the R152K mutation confers resistances in influenza B background [77, 78]. The residue alterations are consistent with the experimental results of Yen et al. [19] where a lower enzymatic activity has been observed with a significant reduction of viral viability [19, 79]. In addition, our simulated results indicate that the R152I, D198N or I222V mutation can enhance the interactions with the OC *N*-acetylamino group (Fig. 2c). The H274Y, E276D, E277G and N294S mutations have been studied before [15, 19, 65, 80–82]. The RMSF plots in

Table 2 The binding energies (ΔE) and binding free energies (ΔG) of oseltamivir carboxylate (OC) with the wild-type and mutated N2 proteins

	ΔE_{ele}	ΔE_{vdW}	ΔG_{sur}	ΔG_{PB}	ΔG_{bind}
WT	−113.8 ± 3.5	−13.6 ± 1.3	−3.8 ± 0.01	113.1 ± 2.6	−18.1 ± 1.5
R118K[a]	–	–	–	–	–
R292K	−110.3 ± 2.0	−24.5 ± 0.4	−3.6 ± 0.01	126.3 ± 2.2	−12.1 ± 1.0
R371K	−125.4 ± 2.9	−24.7 ± 1.1	−4.6 ± 0.02	147.9 ± 3.1	−6.8 ± 1.8
E425G	−202.8 ± 3.2	−25.4 ± 1.2	−4.8 ± 0.01	208.6 ± 3.1	−24.4 ± 2.0
E119D	−232.4 ± 3.2	−22.6 ± 1.2	−4.3 ± 0.02	217.1 ± 2.4	−42.1 ± 2.1
E119V	−135.4 ± 2.8	−20.5 ± 0.9	−4.1 ± 0.02	143.7 ± 2.2	−16.3 ± 1.3
E119A	−193.6 ± 3.8	−28.1 ± 1.1	−4.5 ± 0.02	211.2 ± 4.1	−15.0 ± 3.6
E119G	−122.8 ± 3.6	−15.6 ± 1.4	−3.8 ± 0.02	127.8 ± 2.6	−14.3 ± 1.6
D151E	−159.9 ± 3.3	−20.4 ± 0.9	−4.3 ± 0.02	164.5 ± 2.4	−20.0 ± 1.3
D151N	−105.2 ± 2.0	−30.0 ± 0.5	−4.6 ± 0.02	130.2 ± 2.1	−9.6 ± 1.5
R152K	−184.4 ± 3.1	−19.7 ± 0.9	−4.1 ± 0.03	190.5 ± 3.1	−17.8 ± 2.0
R152I	−177.2 ± 3.0	−31.4 ± 1.9	−5.0 ± 0.02	175.8 ± 3.3	−37.7 ± 2.3
D198N	−116.1 ± 2.8	−34.2 ± 1.1	−5.1 ± 0.02	143.1 ± 3.1	−12.4 ± 3.3
I222V	−175.8 ± 3.0	−25.1 ± 1.2	−4.2 ± 0.01	177.6 ± 2.6	−27.5 ± 1.4
H274Y	−192.4 ± 3.7	−34.6 ± 1.1	−4.8 ± 0.02	189.4 ± 3.1	−42.4 ± 2.3
E276D	−219.9 ± 4.5	−18.5 ± 1.6	−4.5 ± 0.02	204.2 ± 3.4	−38.6 ± 2.2
E277G	−158.2 ± 3.1	−30.1 ± 0.5	−4.7 ± 0.02	173.4 ± 4.0	−19.6 ± 3.8
N294S	−193.8 ± 4.4	−22.4 ± 1.4	−4.4 ± 0.01	189.8 ± 2.7	−30.7 ± 2.2

All values are given in kcal mol^{-1}, and behind "±" are their standard deviations (SD)

[a] OC is far away from the $N2^{R118K}$ active site

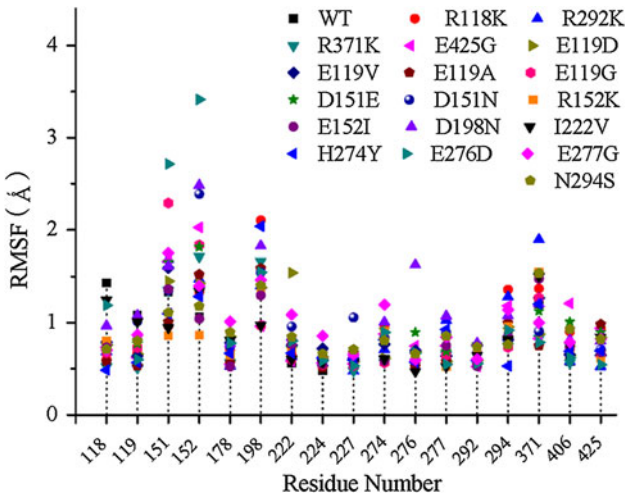

Fig. 3 The root-mean-square fluctuations (*RMSF*) per key active-site residue of the wild-type and mutated N2 proteins complexed with OC

Figs. 3 and S4 show that E276D and N294S mutations cause conformational instabilities to related residues and further to OC orientations, with the ligand-RMSD values equaling 5.1 and 11.3 Å, respectively (Figure S5). Owing to the elongation of the side chain, the H274Y mutation forces the E276 carboxylate anion towards the N2 active site by approximately 4.0 Å, and as a result, the hydrophobic pocket composed of residues E276 and E277 will shrink, thus inducing the OC phenyl ether group to move towards the opposite zone (Fig. 6a). These are consistent with the crystal structure (PDB ID: 3CL0 [65]) and MD simulated results of N1 background [15, 21, 81, 82]. The E276D mutation causes the C_ζ atom to migrate by approximately 4.4 Å, while the hydrophobic pocket alters slightly and can still accommodate the OC pentyl group (Figs. 2d, 6b). This may provide the reason why this mutation causes slight OC resistances [19] and the reduction only in the length of side chain (i.e., from $–CH_2CH_2COOH$ to $–CH_2COOH$) can alter the binding of drugs [66]. The E277G mutation is in a similar situation (Figs. 2d, 6c), and the C_ζ shift amounts to 4.1 Å. The N294S mutation induces OC to depart from the N2 active site. Residue E276 is forced to move towards the active site by the S294 hydroxyl group by 2.0 Å (Figs. 2d, 6d), consistent with the results of N1 background [15, 65].

The calculated binding affinities as compared to experiments

The binding free energies (ΔG_{bind}) of OC–$N2^{WT}$, OC–$N2^{R292K}$ and OC–$N2^{R371K}$ are calculated using the various schemes in "Binding free energies" section and the results are listed in Table S1. Note that ΔG_S refers to the inclusion of entropic contributions ($T\Delta S$). As compared to the default 1 ns MD simulations, the increase of simulation

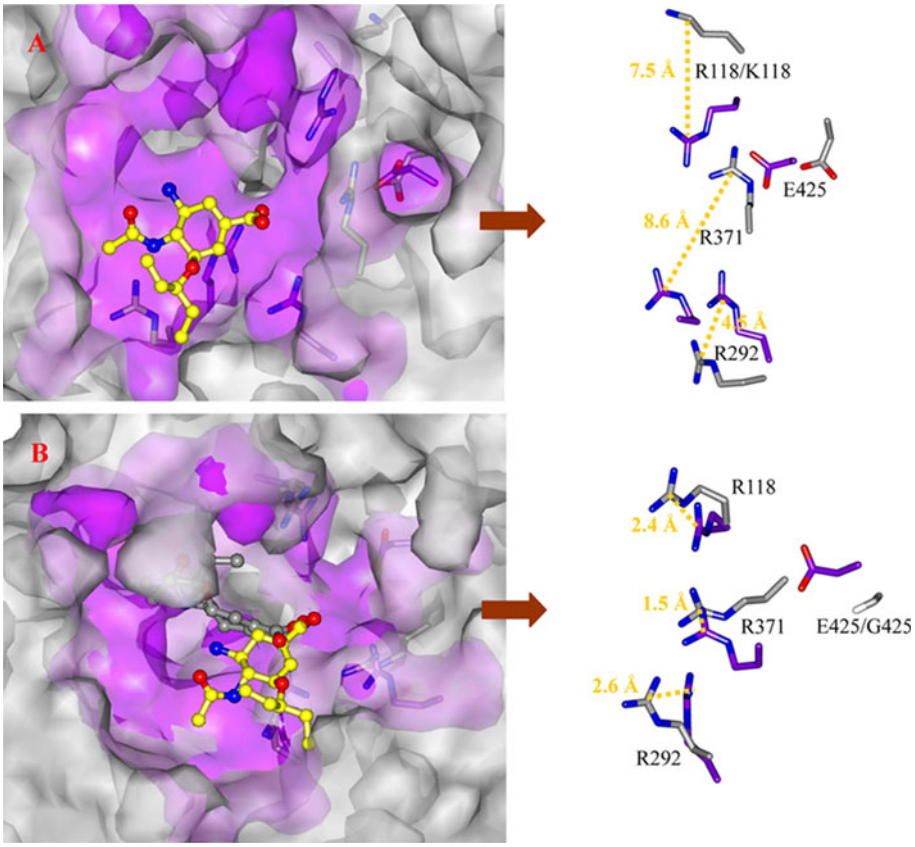

Fig. 4 Equilibrium structures of OC in **a** $N2^{R118K}$ and **b** $N2^{E425G}$. The Connolly surfaces of mutated proteins (in *grey*) are created using the InsightII 2005 scripts, while the active-site surface of $N2^{WT}$ is superposed in *purple*. The C atoms of OC are *colored* in *grey* and *yellow* for the mutated and wild-type docked complexes, and the C, N and O atoms of the mutated active sites are *colored* in *grey*, *blue* and *red*, respectively. In $N2^{R118K}$, the OC ligand moves far from the active site and is not shown

time to 5 ns produces close binding free energies (ΔG_{bind}), and the largest deviation exists in the case of OC–$N2^{R371K}$, where the ΔG_{bind} values are equal to -6.8 ± 1.8 and -3.1 ± 1.4 kcal mol^{-1} for the 1 ns and 5 ns MD simulations, respectively. The deviations of the other two are significantly smaller and below 1.0 kcal mol^{-1}. The fine agreement between the 1 ns and 5 ns MD simulations is due to that the binding free energy calculations are based on the docked structures that have been sufficiently equilibrated by 10 ns MD simulations. The interior dielectric constants have an inconspicuous impact on the binding free energies (ΔG_{bind}), because in all the three cases, the ΔG_{bind} differences for two interior dielectric constants ($\varepsilon_{in} = 1.0$ and 2.0) are less than 1.0 kcal mol^{-1}. In contrast, the explicit water molecules cause a pronounced effect and the binding free energies (ΔG_{bind}) can be even more than threefold with addition of the explicit water molecules; e.g., the ΔG_{bind} value of OC–$N2^{R371K}$ increases from -3.1 ± 1.4 to -11.3 ± 1.2 kcal mol^{-1}. Such clear changes can also be observed by inclusion of entropic contributions ($T\Delta S$). Take OC–$N2^{WT}$ for example. The ΔG_{bind} and ΔG_S values are calculated to be -18.1 ± 1.5 and 1.7 ± 3.5 kcal mol^{-1} for the default 1 ns MD simulations, -17.7 ± 0.9 and 2.1 ± 2.9 kcal mol^{-1} for the 5 ns MD simulations, -34.4 ± 1.1 and -14.6 ± 3.1 kcal mol^{-1} with addition of explicit water molecules as well as -17.8 ± 1.2 and 2.0 ± 3.2 kcal mol^{-1} by change of the interior dielectric constant (ε_{in}) from 1.0 to 2.0, respectively (Table S1). Nonetheless, the 1 ns or 5 ns MD simulations with the default conditions can arrive to comparable results with the experiments at -12.0 kcal mol^{-1} [13], probably due to the counteraction of different effects. In addition, neglect of these effects will not affect the ranking order of the binding free energies, and for all the involved schemes in "Binding free energies" section, the binding free energy differences between the mutated versus wild-type complexes are rather close to each other, see the data in parentheses of Table S1. Accordingly, the default 1 ns MD simulations will be used for the binding free energies unless otherwise noted.

The MM/PBSA methodology has been used to calculate the binding free energies of OC to the wild-type and mutated N2 proteins. For a given ligand (e.g., OC in this work), the NA proteins with larger binding energies (ΔG_{bind}) generally show higher enzymatic activities, and several exceptions due to mutations will be discussed in "Docking of OC to other NA subtypes" section. Table 2 lists the energy contributions from the solutes and solvents. The mutations disturb the electrostatic components ($\Delta E_{ele} + \Delta G_{PB}$) and vdW interactions ($\Delta E_{vdW}$) more than the nonpolar free energy of solvation (ΔG_{sur}). As compared to the wild type, most mutants (except R292K and D151N)

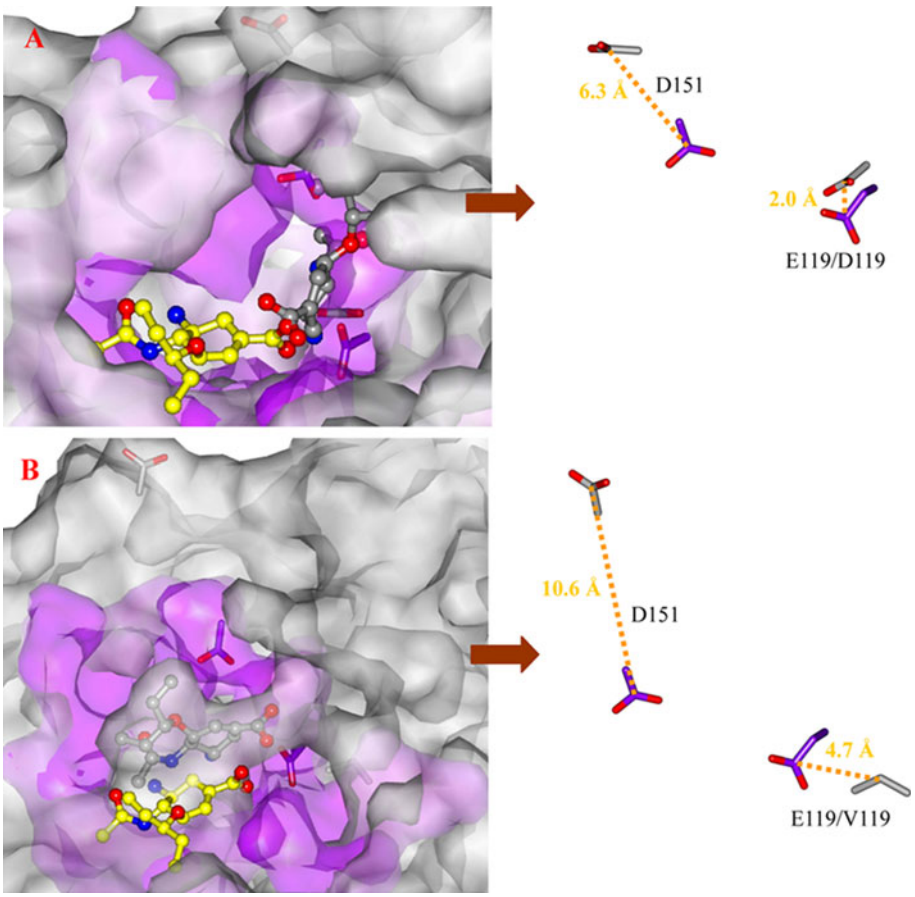

Fig. 5 Equilibrium structures of OC interacting with **a** $N2^{E119D}$ and **b** $N2^{E119V}$. The Connolly surfaces of mutated proteins (in *grey*) are created using the InsightII 2005 scripts, while the active-site surface of $N2^{WT}$ is superposed in *purple*. The C atoms of OC are *colored* in *grey* and *yellow* for the mutated and wild-type docked complexes, and the C, N and O atoms of the mutated active sites are *colored* in *grey*, *blue* and *red*, respectively

have more negative ΔE_{ele} values (especially E119D, -232.4 ± 3.2 vs. -113.8 ± 3.5 kcal mol^{-1}) and more positive ΔG_{PB} values (e.g., E119A, 211.2 ± 4.1 vs. 113.1 ± 2.6 kcal mol^{-1}). These are associated with the conformational changes of the docked complexes. The ΔE_{ele} components are the main driving force for the binding processes, which is consistent with the previous studies [15, 63]. The binding free energies of all the mutants except three differ from the wild type mainly in the electrostatic contributions ($\Delta E_{ele} + \Delta G_{PB}$). As indicated in Tables 1, 2 and Figure S8, more H-bonds in the docked complexes are generally beneficial to the ΔE_{ele} component and binding free energies (ΔG_{bind}). Accordingly, H-bonds should be listed as one important factor to measure the binding quality of NA-ligand complexes and design the potent broad-spectrum NAIs with minimal resistances.

One of the main advantages of the MM/PBSA method is to allow ranking the binding free energies of the various docked complexes. The binding free energies of OC with $N2^{R292K}$ and $N2^{R371K}$ are respectively calculated at -12.1 ± 1.0 and -6.8 ± 1.8 kcal mol^{-1}, in good agreement with the OC-resistances of the inhibitor sensitivity assays (IC_{50} values) [19]. The binding affinity of OC with $N2^{E425G}$ increases to -24.4 ± 2.0 kcal mol^{-1} and disagree with the inhibitor sensitivity assays [69], which may be caused by the used force-fields or calculation protocols (such as GB vs. PB) as previously discussed [32, 64]. In accordance with structural analysis, the binding free energy of the E119D mutation demonstrates that the appropriate side chain length plays an important role during the stabilization of the catalytic residue D151. The order of the related binding affinities is consistent with that of the NAI sensitivity experiments [16, 17, 83]. The binding free energies of $N2^{D151E}$ and $N2^{D151N}$ are equal to -20.0 ± 1.3 and -9.6 ± 1.5 kcal mol^{-1}, which are comparable to the experimental results of the NAI sensitivity and NA enzymatic activity [19]. The binding free energies of the R152K and D198N mutations at -17.8 ± 2.0 and -12.4 ± 3.3 kcal mol^{-1} indicate slight resistances, whereas the R152I and I222V mutations relieve the susceptibility of N2 against OC and thus increase the binding free energies to -37.7 ± 2.3 and -27.5 ± 1.4 kcal mol^{-1}, which are consistent with the increase of enzymatic activities observed experimentally [19, 79]. The binding free energies of H274Y, E276D and N294S are larger than that of the wild type and seem to contradict with the inhibition results [19, 69], which will be discussed in

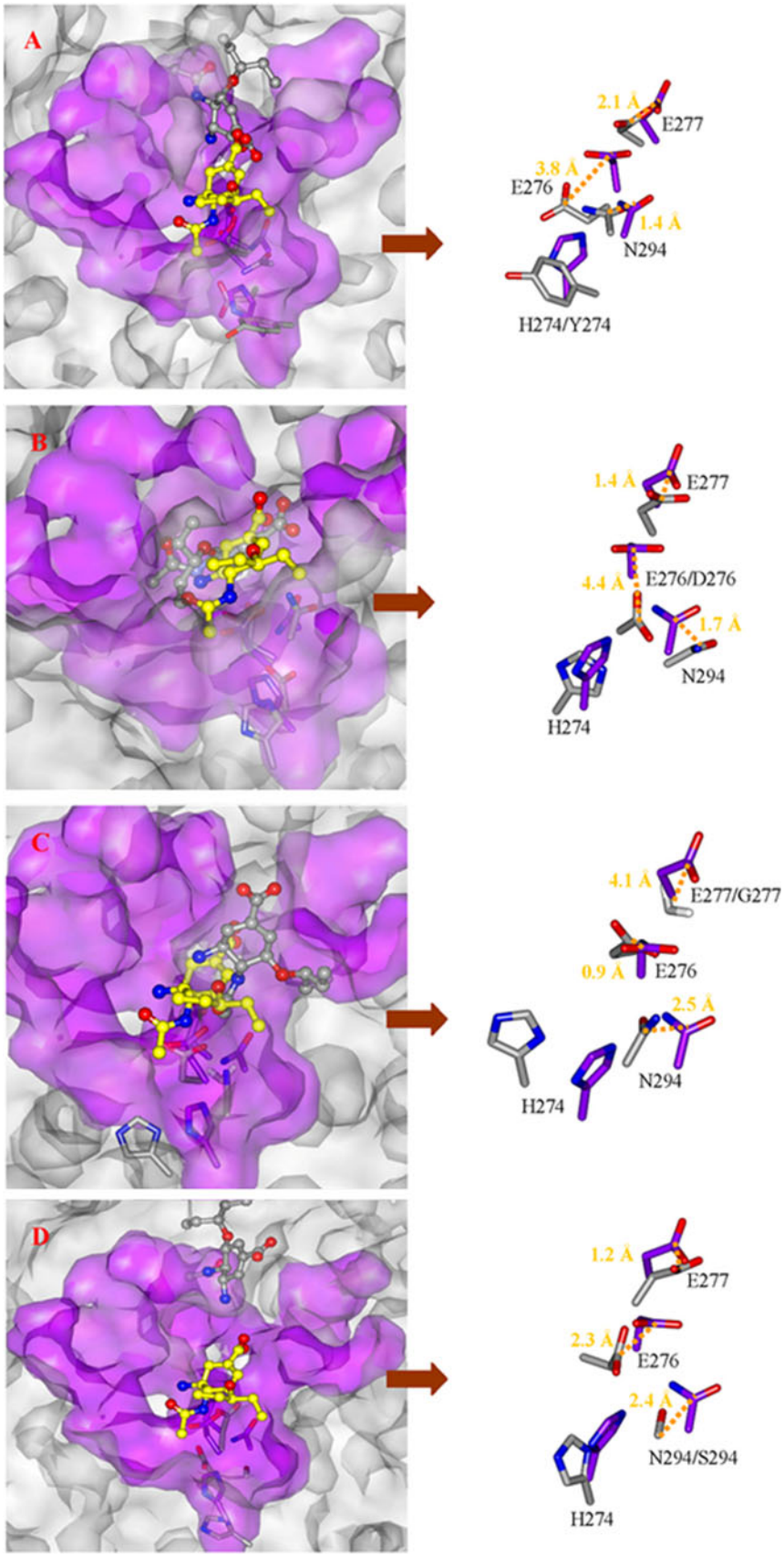

Fig. 6 Equilibrium structures of OC interacting with **a** $N2^{H274Y}$, **b** $N2^{E276D}$, **c** $N2^{E277G}$ and **d** $N2^{N294S}$. The Connolly surfaces of mutated proteins (in *grey*) are created using the InsightII 2005 scripts, while the active-site surface of $N2^{WT}$ is superposed in *purple*. The C atoms of OC are *colored* in *grey* and *yellow* for the mutated and wild-type docked complexes, and the C, N and O atoms of the mutated active sites are *colored* in *grey*, *blue* and *red*, respectively

Table 3 The backbone root-mean-square deviations (RMSD, Å) for the active sites of the binding complexes of OC with various mutated NA-subtypes

	OC–N2	OC–N1	OC–N9	OC–B
R118K	3.0			
R292K	2.2			
R371K	2.3			
E425G	2.2			
E119D	1.7			2.9
E119V	3.3			
E119A	2.0			2.6
E119G	2.0		1.1	2.0
D151E	2.7			2.2
D151N	2.3			
R152K	2.3			2.3
R152I	2.2			
D198N	2.6			2.2
I222V	2.4			
H274Y	1.8	2.7	1.1	1.8
E276D	3.7			
E277G	2.1			
N294S	2.0	2.2		

A subset of 18 residues (118–119, 151–152, 178, 179, 198, 222, 224, 227, 274, 276–277, 292, 294, 371, 406 and 425) is used to calculate the RMSDs (according to N2 numbering)

The wild types are used as the benchmarks

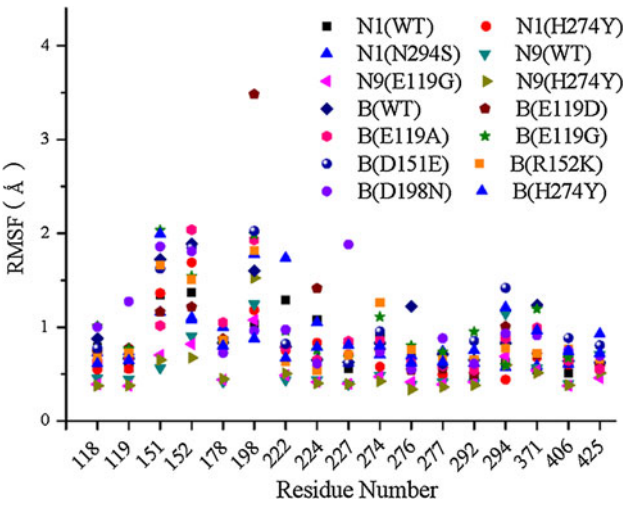

Fig. 7 The root mean square fluctuations (*RMSF*) per key active-site residue for B-type and N1-, N9-subtype NA proteins complexed with OC. The residue numbering is in accord with N2

"Docking of OC to other NA subtypes" section. The activity experiments show that the E276D mutation has a high enzymatic activity (95.4 ± 43.9 pmol/30 min ng^{-1}) although significantly less than the wild type (2,861.4 ± 107.2 pmol/30 min ng^{-1}) [15, 84–86]. In addition, the binding free energies for these variants rank in the same order as those determined by the NAI sensitivity assays [16, 17, 83, 87]. The order of the related binding affinities is consistent with that of the NAI sensitivity experiments.

Docking of OC to other NA subtypes

In addition to the N2 subtype, the resistances to oseltamivir are detected in other influenza viruses, and a few resistant mutants have occurred during clinical trials [5, 13, 14]. The interactions of OC with the N1-, N9-subtype and B-type NA proteins are also investigated to find clues for design of potent broad-spectrum NA inhibitors with minimal resistances. The time-evolution backbone RMSDs in Figure S9 indicate that the average structures of the 5–10 ns MD trajectories are suitable for analysis. The backbone RMSD values in Table 3 and RMSF plots in Figs. 7 and S10 show that these mutations cause conformational fluctuations to the key active-site residues [11–17], and similar conformational alterations are observed for the four NA subtypes (N1, N2, N9 and B). As the MD simulations indicate, the E119 carboxylate group plays an important role during ligand binding by interactions with the OC amino and *N*-acetylamino moieties, which will disappear due to the E119V/A/G mutation and agree with the decrease of binding affinities observed in several strains of influenza viruses A and B [11–17, 69]. For N2 subtype or B type, residue R152 in the wild type has interaction with residue D198 forming an H-bond with the OC *N*-acetylamino group, and the R152K mutation alters the two residues and causes the non-existence of this H-bond, which may further result in the slight OC resistances [77, 78].

The binding differences among the various NA subtypes can be detected by a more in-depth analysis and should be responsible for the subtype-specific drug resistances [11–17, 69]. Table 4 lists the binding energies of OC with the various NA subtypes. The binding energies are generally in good agreement with the enzymatic activities; nonetheless, exceptions can be found in the mutations (H274Y and N294S) where the OC interaction modes are significantly different from the wild type. In these cases, the ligands will interact with residues R430, Q136, V149 and Q347 that normally are not involved during the binding. For example, the interaction energies of residue R430 with the $N1^{H274Y}$, $N2^{H274Y}$ $N9^{H274Y}$ and B^{H274Y} proteins are calculated to be as large as −14.8 (−0.02), −62.3 (−0.00), −73.4 (−0.00) and −13.5 (−0.03) kcal mol^{-1}, respectively. Note that the data in parentheses are for the corresponding wild-type proteins. The unwanted interaction energies are not beneficial to the ligand binding and therefore cause the apparent "disagreement" with the experimental observations.

Table 4 The binding energies (ΔE) of OC with N1, N2, N9 and B (wild-type and mutated)

	N1		N2		N9		B	
	ΔE_{ele}	ΔE_{vdW}	ΔE_{ele}	ΔE_{vdW}	ΔE_{ele}	ΔE_{vdW}	ΔE_{ele}	ΔE_{vdW}
WT	−214.3	−29.8	−629.0	−25.1	−678.1	−1.6	−163.5	−29.6
E119D			−754.8	−23.3			−173.5	−23.6
E119A			−569.1	−22.5			−96.9	−26.6
E119G			−492.0	−11.3	−500.4	−8.1	−161.3	−30.0
D151E			−678.2	−27.6			−215.4	−29.6
R152K			−616.5	−23.9			−206.1	−22.9
D198N			−418.7	−21.8			−215.7	−25.6
H274Y	−248.0	−26.1	−673.4	−28.8	−727.6	5.1	−197.9	−35.6
N294S	−232.5	−17.7	−753.6	−39.7				

All values are given in kcal mol^{-1}, obtained by the Dock module (InsightII 2005)

As shown in Figs. 6a and 8, the H274Y mutations cause the OC phenyl ether moiety to departure somewhat from the NA active sites [15]. The substitution of H274 by a bulkier Y274 forces the carboxylate group of residue E276 to move towards the NA active site center. This hampers residue E276 from rotating to the correct conformation that will interact with R224 [65], associated with the obvious reduction of the hydrophobic pocket (residues E276 and E277). As compared to the wild types, the C_ζ atoms of residue E276 in the H274Y mutations migrate by 2.1 Å for N1, 3.8 Å for N2, 3.6 Å for N9 and 3.1 Å for B, respectively. For N1 background, the OC resistances should be caused by the unfavorable orientation of residue E276 (Figs. 7, 8) [15, 21, 65, 88]. As discussed in "The mutagenesis analysis" section, residue E276 in the wild type should undergo conformational rearrangement in order to match the bulky side chain of OC; however, this rearrangement has been inhibited by the $N1^{H274Y}$ mutation. In addition, the $N1^{H274Y}$ mutation alters the R292 position (C_ζ: 1.8 Å) and further disrupts the accommodation of the OC pentyl moiety in the hydrophobic pocket comprising residues E276, E277 and N294; meanwhile, the salt bridge between residue R292 and the OC carboxylate anion has been destroyed [15, 21, 88]. However, the rearrangement of residue R292 (C_ζ: 0.9 Å) has not been observed in $N2^{H274Y}$ (Figs. 3, 6), with only slight rotation of residue E276 towards residue R224 (C_ζ–C_ζ: 5.0 Å), explaining why the $N2^{H274Y}$ virus does not result in the OC resistances [69, 89]. The migration distances of residue R292 are nearly the same for the N2 and N9 subtypes, probably due to their sequence (50 %) and structure similarities [5, 21]. The resistant mutants such as E119D/V/A/G and R292K have been observed for both N2 and N9 subtypes, which further demonstrates the consistency between these two NA subtypes [11, 15–19].

For the N1-, N9-subtypes and B-type NA proteins, the electrostatic (ΔE_{ele}) rather than vdW (ΔE_{vdW}) interactions

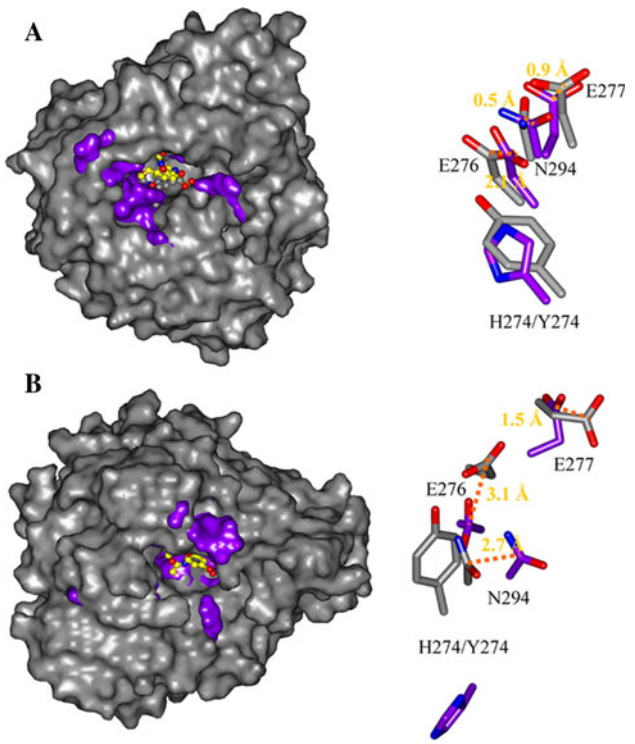

Fig. 8 Equilibrium structures of OC interacting with **a** $N1^{H274Y}$ and **b** B^{H274Y}. The Connolly surfaces of mutated proteins (in *grey*) are created using the InsightII 2005 scripts, while the active-site surfaces of the wild type ($N1^{WT}$ and B^{WT}) are superposed in *purple*. The C atoms of OC are *colored* in *grey* and *yellow* for the mutated and wild-type docked complexes, and the C, N and O atoms of the mutated active sites are *colored* in *grey*, *blue* and *red*, respectively. The residue *numbering* of the protein is in accordance with N2

are mainly responsible for the binding differences between the mutants and wild types (Table 4). This is in agreement with the situation of the N2 subtype discussed above. For example, the ΔE_{ele} value of OC–$N9^{E119G}$ is equal to −500.4 kcal mol^{-1} and far less than the wild type (−678.1 kcal mol^{-1}); instead, the ΔE_{vdW} change is much

less obvious, and the values are small for both wild type and mutant (−1.6 vs. −8.1 kcal mol^{-1}) [11–17]. As compared to the wild type, the H274Y mutations alter the ΔE_{ele} (ΔE_{vdW}) values by −33.7 (3.7), −44.4 (−3.7), −49.5 (6.7) and −34.4 (−6.0) kcal mol^{-1} for the N1, N2, N9 and B subtypes, respectively (Table 4). It can be seen that the ΔE_{vdW} changes account for only 11.0, 8.3, 13.5 and 17.4 % of the corresponding ΔE_{ele} changes. The interactions of OC with the surrounding NA residues are analyzed. It indicates that for the different NA subtypes, the ΔE_{ele} differences among them are mainly caused by the conserved residues at the active sites, which further results in the subtype-specific drug resistances. It supports the hypothesis that the NA pocket region is an important target site and the NA ligands structurally close to the native substrate (sialic acid) are generally robust to the NA proteins because of similar interactions [5, 15, 19, 65, 72, 80–82].

Conclusions

The screening for susceptibility of influenza viruses has detected oseltamivir-resistant NA variants. To promote the design of broad-spectrum NA inhibitors with minimal resistances and understanding of subtype-specific drug resistances, the flexible docking, MD and binding (free) energy calculations within explicit water solvent were performed on the N1-, N2-, N9-subtype and B-type NA backgrounds. Meanwhile, this work also provides useful insights for the mutation effects on protein conformations and interaction mechanisms with ligands.

The mutation rates of the N2 active-site residues were calculated with the aid of platform in Influenza Research Database (IRD). It showed that the catalytic R118, R152, E276, R292, R371 and framework E119, D198, I222, H274, E277, N294, E425 residues are relatively conserved while the catalytic D151 residue is likely to mutate. The MD simulations indicated that each mutation causes conformational alterations to NA active sites and position shifts of all the key residues, requiring much longer time to equilibrate than the wild types. The NA active sites are reduced by the R118K, E119G, R152I, D198N, E276D, N294S, R371K and E425G mutations whereas enlarged by the E119D/V/A, D151E/N, R152K, I222V, H274Y, E277G and R292K mutations. As a result of the conformation alterations, the binding properties will be deviated, but larger alterations do not necessarily correspond to greater deviations to the ligand binding properties.

The systematic studies of the N2 subtype showed that the mutated residues affect strongly the nearby residues and further the conformations of the active sites. The different effects of all the potential mutations (R118K, E119A, E119D, E119G, E119V, D151E, D151N, R152I, R152K, D198N, I222V, H274Y, E276D, E277G, N294S, R292K, R371K and E425G) have been discussed. For example, mutations of the arginine triad (R118, R292 and R371) indicated that among them, residue R118 plays the largest role during ligand binding albeit all of them are known to be important. Owing to the mutation of R118, the ligand moves far from the N2 active site and all H-bonds that are present in the wild type have been destroyed. The mutations of E119 demonstrated its negative charges and suitable side chain lengths are crucial to stabilize the catalytic D151, whose significant role has been explored as well. Generally, the binding free energies calculated using the MM/PBSA method is in good agreement with the experimental results. It explains why the R152K and D198N mutations confer resistances to OC. Susceptibility of influenza virus to NA inhibitors can be reinforced by some mutations; e.g., the binding free energies of OC with N2 due to the E119D mutation increase from −18.1 ± 1.5 to −42.1 ± 2.1 kcal mol^{-1}.

The mutations result in similar changes on the active-site conformations and binding properties for the various NA subtypes, which explains frequent cross resistances observed by the in vitro experiments and reverse genetics. On the other hand, differences albeit not obvious can be detected for the various NA subtypes and should be responsible for the subtype-specific resistances, which is clarified mainly using the H274Y mutation. The exceptional agreements of the N2 and N9 subtypes in the OC-resistant mutants are caused by their sequence and structure similarities. For all NA subtypes, the electrostatic components ($\Delta E_{ele} + \Delta G_{PB}$) are the major driving force for ligand binding and also largely responsible for the binding differences between the wild-type and mutated NA proteins.

Acknowledgments We are grateful for the financial supports from the National Natural Science Foundations (No. 20903019, 31200429), Special Fund for Basic Scientific Research of Central Colleges (SWU113049) and Scientific Research Foundation of Heilongjiang Provincial Education Department (No. 12531690). We show sincere gratitude to Prof. David A. Case for authorizing the use of the Amber 11 software and Shanghai Supercomputing Center for the computing time.

References

1. Layne SP, Monto AS, Taubenberger JK (2009) Pandemic influenza: an inconvenient mutation. Science 323(5921):1560–1561
2. Bautista E, Chotpitayasunondh T, Gao Z, Harper SA, Shaw M, Uyeki TM, Zaki SR, Hayden FG, Hui DS, Kettner JD, Kumar A, Lim M, Shindo N, Penn C, Nicholson KG (2010) Clinical aspects of pandemic 2009 influenza A (H1N1) virus infection. N Engl J Med 362(18):1708–1719
3. Air GM, Laver WG (1989) The neuraminidase of influenza virus. Proteins 6(4):341–356

4. Chong AKJ, Pegg MS, Taylor NR, Vonitzstein M (1992) Evidence for a sialosyl cation transition-state complex in the reaction of sialidase from influenza-virus. Eur J Biochem 207(1):335–343
5. von Itzstein M (2007) The war against influenza: discovery and development of sialidase inhibitors. Nat Rev Drug Discov 6(12):967–974
6. Das K, Aramini JM, Ma LC, Krug RM, Arnold E (2010) Structures of influenza A proteins and insights into antiviral drug targets. Nat Struct Mol Biol 17(5):530–538
7. Moscona A (2008) Medical management of influenza infection. Annu Rev Med 59:397–413
8. Kim CU, Lew W, Williams MA, Liu H, Zhang L, Swaminathan S, Bischofberger N, Chen MS, Mendel DB, Tai CY (1997) Influenza neuraminidase inhibitors possessing a novel hydrophobic interaction in the enzyme active site: design, synthesis, and structural analysis of carbocyclic sialic acid analogues with potent anti-influenza activity. J Am Chem Soc 119(4):681–690
9. Gubareva LV, Kaiser L, Hayden FG (2000) Influenza virus neuraminidase inhibitors. Lancet 355(9206):827–835
10. Jedrzejas MJ, Singh S, Brouillette WJ, Laver WG, Air GM, Luo M (1995) Structures of aromatic inhibitors of influenza virus neuraminidase. Biochemistry 34(10):3144–3151
11. Kiso M, Mitamura K, Sakai-Tagawa Y, Shiraishi K, Kawakami C, Kimura K, Hayden FG, Sugaya N, Kawaoka Y (2004) Resistant influenza A viruses in children treated with oseltamivir: descriptive study. Lancet 364(9436):759–765
12. Moscona A (2005) Oseltamivir resistance—disabling our influenza defenses. N Engl J Med 353(25):2633–2636
13. Aruksakunwong O, Malaisree M, Decha P, Sompornpisut P, Parasuk V, Pianwanit S, Hannongbua S (2007) On the lower susceptibility of oseltamivir to influenza neuraminidase subtype N1 than those in N2 and N9. Biophys J 92(3):798–807
14. Collins PJ, Haire LF, Lin YP, Liu J, Russell RJ, Walker PA, Martin SR, Daniels RS, Gregory V, Skehel JJ, Gamblin SJ, Hay AJ (2009) Structural basis for oseltamivir resistance of influenza viruses. Vaccine 27(45):6317–6323
15. Wang NX, Zheng JJ (2009) Computational studies of H5N1 influenza virus resistance to oseltamivir. Protein Sci 18(4):707–715
16. McKimm-Breschkin JL (2000) Resistance of influenza viruses to neuraminidase inhibitors–a review. Antiviral Res 47(1):1–17
17. Gubareva LV (2004) Molecular mechanisms of influenza virus resistance to neuraminidase inhibitors. Virus Res 103(1–2):199–203
18. Squires B, Macken C, Garcia-Sastre A, Godbole S, Noronha J, Hunt V, Chang R, Larsen CN, Klem E, Biersack K, Scheuermann RH (2008) BioHealthBase: informatics support in the elucidation of influenza virus host pathogen interactions and virulence. Nucleic Acids Res 36(Database issue):D497–D503
19. Yen HL, Hoffmann E, Taylor G, Scholtissek C, Monto AS, Webster RG, Govorkova EA (2006) Importance of neuraminidase active-site residues to the neuraminidase inhibitor resistance of influenza viruses. J Virol 80(17):8787–8795
20. Rudrawar S, Dyason JC, Rameix-Welti MA, Rose FJ, Kerry PS, Russell RJ, van der Werf S, Thomson RJ, Naffakh N, von Itzstein M (2010) Novel sialic acid derivatives lock open the 150-loop of an influenza A virus group-1 sialidase. Nat Commun 1:113
21. Russell RJ, Haire LF, Stevens DJ, Collins PJ, Lin YP, Blackburn GM, Hay AJ, Gamblin SJ, Skehel JJ (2006) The structure of H5N1 avian influenza neuraminidase suggests new opportunities for drug design. Nature 443(7107):45–49
22. Smith BJ, Colman PM, Von Itzstein M, Danylec B, Varghese JN (2001) Analysis of inhibitor binding in influenza virus neuraminidase. Protein Sci 10(4):689–696
23. Taylor NR, Cleasby A, Singh O, Skarzynski T, Wonacott AJ, Smith PW, Sollis SL, Howes PD, Cherry PC, Bethell R, Colman P, Varghese J (1998) Dihydropyrancarboxamides related to zanamivir: a new series of inhibitors of influenza virus sialidases. 2. Crystallographic and molecular modeling study of complexes of 4-amino-4H-pyran-6-carboxamides and sialidase from influenza virus types A and B. J Med Chem 41(6):798–807
24. Yang ZW, Yang G, Zu YG, Fu YJ, Zhou LJ (2009) The conformational analysis and proton transfer of the neuraminidase inhibitors: a theoretical study. Phys Chem Chem Phys 11:10035–10041
25. Yang Z, Nie Y, Yang G, Zu Y, Fu Y, Zhou L (2010) Synergistic effects in the designs of neuraminidase ligands: analysis from docking and molecular dynamics studies. J Theor Biol 267(3):363–374
26. Yang ZW, Zu YG, Wu XM, Liu CB, Yang G (2010) A computational investigation on the interaction mechanisms of neuraminidases and 3-(3-pentyloxy)benzoic acid. Acta Chimi Sin 14:1370–1378
27. Yang ZW, Wu XM, Zu YG, Yang G, Zhou LJ (2012) Understanding the chiral recognitions between neuraminidases and inhibitors: studies with DFT, docking and MD methods. Int J Quantum Chem 112(3):909–921
28. InsightII Molecular Modeling Program Package (2005) Accelrys, San Diego, CA
29. Hess B, Kutzner C, van der Spoel D, Lindahl E (2008) GROMACS 4: algorithms for highly efficient, load-balanced, and scalable molecular simulation. J Chem Theory Comput 4:435–447
30. Jorgensen WL, Tirado-Rives J (1988) Energy minimization for crystals of cyclic peptides and crambin. J Am Chem Soc 110:1657–1666
31. Jorgensen WL, Maxwell DS, Tirado-Rives J (1996) Development and testing of the OPLS all-atom force field on conformational energetics and properties of organic liquids. J Am Chem Soc 118:11225–11236
32. Pickholz M, Oliveira ON Jr, Skaf MS (2007) Interactions of chlorpromazine with phospholipid monolayers: effects of the ionization state of the drug. Biophys Chem 125(2–3):425–434
33. Berendsen HJC, Postma JPM, van Gunsteren WF, Hermans J (1981) Interaction models for water in relation to protein hydration. In: Pullman B (ed) Intermolecular forces Dordrecht. Reidel, Dordrecht, pp 331–342
34. Berendsen HJC, Postma JPM, van Gunsteren WF, DiNola A, Haak JR (1984) Molecular dynamics with coupling to an external bath. J Chem Phys 81(8):3684–3690
35. Darden T, York D, Pedersen L (1993) Particle mesh Ewald: an N [center-dot] log(N) method for Ewald sums in large systems. J Chem Phys 98(12):10089–10092
36. Hess B, Bekker H, Berendsen HJC, Fraaije JGEM (1997) LINCS: a linear constraint solver for molecular simulations. J Comput Chem 18(12):1463–1472
37. Mai BK, Viet MH, Li MS (2010) Top leads for swine influenza A/H1N1 virus revealed by steered molecular dynamics approach. J Chem Inf Model 50(12):2236–2247
38. Affinity User Guide (2005) Accelrys Inc., San Diego, CA, USA
39. Frisch MJ, Trucks GW, Schlegel HB, Scuseria GE, Robb MA, Cheeseman JR, Montgomery JA, Vreven T Jr, Kudin KN, Burant JC, Millam JMI, Tomasi J, Barone V, Mennucci B, Cossi M, Scalmani G, Rega N, Petersson GA, Nakatsuji H, Hada M, Ehara M, Toyota K, Fukuda R, Hasegawa J, Ishida M, Nakajima T, Honda Y, Kitao O, Nakai H, Klene M, Li X, Knox JE, Hratchian HP, Cross JB, Adamo C, Jaramillo J, Gomperts R, Stratmann RE, Yazyev O, Austin AJ, Cammi R, Pomelli C, Ochterski JW, Ayala PY, Morokuma K, Voth GA, Salvador P, Dannenberg JJ, Zakrzewski VG, Dapprich S, Daniels AD, Strain MC, Farkas O, Malick DK, Rabuck AD, Raghavachari K, Foresman JB, Ortiz JV, Cui Q, Baboul AG, Clifford S, Cioslowski J, Stefanov BB,

Liu G, Liashenko A, Piskorz P, Komaromi I, Martin RL, Fox DJ, Keith T, Al-Laham MA, Peng CY, Nanayakkara A, Challacombe M, Gill MW, Johnson B, Chen W, Wong MW, Gonzalez C, Pople JA (2004) Gaussian 03. Revision D.01, Gaussian, Inc., Wallingford CT

40. Yang ZW, Wu XM, Zhou LJ, Yang G (2009) A proline-based neuraminidase inhibitor: DFT studies on the zwitterion conformation, stability and formation. Int J Mol Sci 10(9):3918–3930
41. Jorgensen WL, Chandrasekhar J, Madura JD, Impey RW, Klein ML (1983) Comparison of simple potential functions for simulating liquid water. J Chem Phys 79:926–935
42. Berendsen HJC, van der Spoel D, van Drunen R (1995) GROMACS: a message-passing parallel molecular dynamics implementation. Comput Phys Commun 91(1–3):43–56
43. Gohlke H, Case DA (2004) Converging free energy estimates: MM-PB(GB)SA studies on the protein–protein complex Ras–Raf. J Comput Chem 25(2):238–250
44. Case DA, Darden TA, Cheatham TE III, Simmerling CL, Wang J, Duke RE, Luo R, Walker RC, Zhang W, Merz KM, Roberts B, Wang B, Hayik S, Roitberg A, Seabra G, Kolossváry I, Wong KF, Paesani F, Vanicek J, Liu XW, Brozell SR, Steinbrecher T, Gohlke H, Cai Q, Ye X, Wang J, Hsieh MJ, Cui G, Roe DR, Mathews DH, Seetin MG, Sagui C, Babin V, Luchko T, Gusarov S, Kovalenko A, Kollman PA (2010) AMBER11. University of California, San Francisco
45. Kuhn B, Gerber P, Schulz-Gasch T, Stahl M (2005) Validation and use of the MM-PBSA approach for drug discovery. J Med Chem 48(12):4040–4048
46. Duan Y, Wu C, Chowdhury S, Lee MC, Xiong G, Zhang W, Yang R, Cieplak P, Luo R, Lee T, Caldwell J, Wang J, Kollman P (2003) A point-charge force field for molecular mechanics simulations of proteins based on condensed-phase quantum mechanical calculations. J Comput Chem 24(16):1999–2012
47. Bonnet P, Bryce RA (2004) Molecular dynamics and free energy analysis of neuraminidase-ligand interactions. Protein Sci 13(4):946–957
48. Bonnet P, Bryce RA (2005) Scoring binding affinity of multiple ligands using implicit solvent and a single molecular dynamics trajectory: application to influenza neuraminidase. J Mol Graph Model 24(2):147–156
49. Sitkoff D, Sharp KA, Honig B (1994) Accurate calculation of hydration free energies using macroscopic solvent models. J Phys Chem 98(7):1978–1988
50. Hou T, Wang J, Li Y, Wang W (2011) Assessing the performance of the MM/PBSA and MM/GBSA methods. 1. The accuracy of binding free energy calculations based on molecular dynamics simulations. J Chem Inf Model 51(1):69–82
51. Kar P, Knecht V (2012) Mutation-induced loop opening and energetics for binding of tamiflu to influenza N8 neuraminidase. J Phys Chem B 116(21):6137–6149
52. Xu L, Sun H, Li Y, Wang J, Hou T (2013) Assessing the performance of MM/PBSA and MM/GBSA methods. 3. The impact of force fields and ligand charge models. J Phys Chem B 117(28):8408–8421
53. Stoll V, Stewart KD, Maring CJ, Muchmore S, Giranda V, Gu Y-GY, Wang G, Chen Y, Sun M, Zhao C, Kennedy AL, Madigan DL, Xu Y, Saldivar A, Kati W, Laver G, Sowin T, Sham HL, Greer J, Kempf D (2003) Influenza neuraminidase inhibitors: structure-based design of a novel inhibitor series. Biochemistry 42(3):718–727
54. Lentz MR, Air GM (1986) Loss of enzyme activity in a site-directed mutant of influenza neuraminidase compared to expressed wild-type protein. Virology 148(1):74–83
55. Wei X, Els MC, Webster RG, Air GM (1987) Effects of site-specific mutation on structure and activity of influenza virus B/Lee/40 neuraminidase. Virology 156(2):253–258
56. Lentz MR, Webster RG, Air GM (1987) Site-directed mutation of the active site of influenza neuraminidase and implications for the catalytic mechanism. Biochemistry 26(17):5351–5358
57. Ghate AA, Air GM (1998) Site-directed mutagenesis of catalytic residues of influenza virus neuraminidase as an aid to drug design. Eur J Biochem 258(2):320–331
58. Herlocher ML, Truscon R, Elias S, Yen HL, Roberts NA, Ohmit SE, Monto AS (2004) Influenza viruses resistant to the antiviral drug oseltamivir: transmission studies in ferrets. J Infect Dis 190(9):1627–1630
59. Yen HL, Herlocher LM, Hoffmann E, Matrosovich MN, Monto AS, Webster RG, Govorkova EA (2005) Neuraminidase inhibitor-resistant influenza viruses may differ substantially in fitness and transmissibility. Antimicrob Agents Chemother 49(10):4075–4084
60. Ho H-T, Hurt AC, Mosse J, Barr I (2007) Neuraminidase inhibitor drug susceptibility differs between influenza N1 and N2 neuraminidase following mutagenesis of two conserved residues. Antivir Res 76(3):263–266
61. Mohan S, Pinto BM (2007) Zwitterionic glycosidase inhibitors: salacinol and related analogues. Carbohydr Res 342(12–13):1551–1580
62. McKimm-Breschkin J, Trivedi T, Hampson A, Hay A, Klimov A, Tashiro M, Hayden F, Zambon M (2003) Neuraminidase sequence analysis and susceptibilities of influenza virus clinical isolates to zanamivir and oseltamivir. Antimicrob Agents Chemother 47(7):2264–2272
63. Masukawa KM, Kollman PA, Kuntz ID (2003) Investigation of neuraminidase-substrate recognition using molecular dynamics and free energy calculations. J Med Chem 46(26):5628–5637
64. Chachra R, Rizzo RC (2008) Origins of resistance conferred by the R292K neuraminidase mutation via molecular dynamics and free energy calculations. J Chem Theory Comput 4(9):1526–1540
65. Collins PJ, Haire LF, Lin YP, Liu J, Russell RJ, Walker PA, Skehel JJ, Martin SR, Hay AJ, Gamblin SJ (2008) Crystal structures of oseltamivir-resistant influenza virus neuraminidase mutants. Nature 453(7199):1258–1261
66. Cheng LS, Amaro RE, Xu D, Li WW, Arzberger PW, McCammon JA (2008) Ensemble-based virtual screening reveals potential novel antiviral compounds for avian influenza neuraminidase. J Med Chem 51(13):3878–3894
67. Gubareva LV, Webster RG, Hayden FG (2001) Comparison of the activities of zanamivir, oseltamivir, and RWJ-270201 against clinical isolates of influenza virus and neuraminidase inhibitor-resistant variants. Antimicrob Agents Chemother 45(12):3403–3408
68. Gong J, Xu W, Zhang J (2007) Structure and functions of influenza virus neuraminidase. Curr Med Chem 14(1):113–122
69. Richard M, Deleage C, Barthelemy M, Lin YP, Hay A, Lina B, Ferraris O (2008) Impact of influenza A virus neuraminidase mutations on the stability, activity, and sensibility of the neuraminidase to neuraminidase inhibitors. J Clin Virol 41(1):20–24
70. Hitaoka S, Harada M, Yoshida T, Chuman H (2010) Correlation analyses on binding affinity of sialic acid analogues with influenza virus neuraminidase-1 using ab initio MO calculations on their complex structures. J Chem Inf Model 50(10):1796–1805
71. Smith BJ, McKimm-Breshkin JL, McDonald M, Fernley RT, Varghese JN, Colman PM (2002) Structural studies of the resistance of influenza virus neuraminidase to inhibitors. J Med Chem 45(11):2207–2212
72. Colman PM (2009) New antivirals and drug resistance. Annu Rev Biochem 78:95–118
73. Kairys V, Gilson MK, Lather V, Schiffer CA, Fernandes MX (2009) Toward the design of mutation-resistant enzyme inhibitors: further evaluation of the substrate envelope hypothesis. Chem Biol Drug Des 74(3):234–245

74. Varghese JN, McKimm-Breschkin JL, Caldwell JB, Kortt AA, Colman PM (1992) The structure of the complex between influenza virus neuraminidase and sialic acid, the viral receptor. Proteins 14(3):327–332
75. Nguyen HT, Fry AM, Gubareva LV (2012) Neuraminidase inhibitor resistance in influenza viruses and laboratory testing methods. Antivir Ther 17(1 Pt B):159–173
76. Orozovic G, Orozovic K, Lennerstrand J, Olsen B (2011) Detection of resistance mutations to antivirals oseltamivir and zanamivir in avian influenza A viruses isolated from wild birds. PLoS ONE 6(1):e16028
77. Gubareva LV, Matrosovich MN, Brenner MK, Bethell RC, Webster RG (1998) Evidence for zanamivir resistance in an immunocompromised child infected with influenza B virus. J Infect Dis 178(5):1257–1262
78. Jackson D, Barclay W, Zurcher T (2005) Characterization of recombinant influenza B viruses with key neuraminidase inhibitor resistance mutations. J Antimicrob Chemother 55(2):162–169
79. Baz M, Abed Y, McDonald J, Boivin G (2006) Characterization of multidrug-resistant influenza A/H3N2 viruses shed during 1 year by an immunocompromised child. Clin Infect Dis 43(12):1555–1561
80. Rungrotmongkol T, Malaisree M, Nunthaboot N, Sompornpisut P, Hannongbua S (2010) Molecular prediction of oseltamivir efficiency against probable influenza A (H1N1-2009) mutants: molecular modeling approach. Amino Acids 39(2):393–398
81. Nguyen TT, Mai BK, Li MS (2011) Study of Tamiflu sensitivity to variants of A/H5N1 virus using different force fields. J Chem Inf Model 51(9):2266–2276
82. Vergara-Jaque A, Poblete H, Lee EH, Schulten K, Gonzalez-Nilo F, Chipot C (2012) Molecular basis of drug resistance in A/H1N1 virus. J Chem Inf Model 52(10):2650–2656
83. Zurcher T, Yates PJ, Daly J, Sahasrabudhe A, Walters M, Dash L, Tisdale M, McKimm-Breschkin JL (2006) Mutations conferring zanamivir resistance in human influenza virus N2 neuraminidases compromise virus fitness and are not stably maintained in vitro. J Antimicrob Chemother 58(4):723–732
84. Amaro RE, Minh DDL, Cheng LS, Lindstrom WM, Olson AJ, Lin J-H, Li WW, McCammon JA (2007) Remarkable loop flexibility in avian influenza N1 and its implications for antiviral drug design. J Am Chem Soc 129(25):7764–7765
85. Amaro RE, Cheng X, Ivanov I, Xu D, McCammon JA (2009) Characterizing loop dynamics and ligand recognition in human- and avian-type influenza neuraminidases via generalized born molecular dynamics and end-point free energy calculations. J Am Chem Soc 131(13):4702–4709
86. Udommaneethanakit T, Rungrotmongkol T, Bren U, Frecer V, Stanislav M (2009) Dynamic behavior of avian influenza A virus neuraminidase subtype H5N1 in complex with oseltamivir, zanamivir, peramivir, and their phosphonate analogues. J Chem Inf Model 49(10):2323–2332
87. Samson M, Pizzorno A, Abed Y, Boivin G (2013) Influenza virus resistance to neuraminidase inhibitors. Antiviral Res 98(2): 174–185
88. Wang MZ, Tai CY, Mendel DB (2002) Mechanism by which mutations at his274 alter sensitivity of influenza a virus n1 neuraminidase to oseltamivir carboxylate and zanamivir. Antimicrob Agents Chemother 46(12):3809–3816
89. Abed Y, Baz M, Boivin G (2006) Impact of neuraminidase mutations conferring influenza resistance to neuraminidase inhibitors in the N1 and N2 genetic backgrounds. Antivir Ther 11(8):971–976